



**HAL**  
open science

## Strong impacts of biomass burning, nitrogen fertilization, and fine particles on gas-phase hydrogen peroxide (H<sub>2</sub>O<sub>2</sub>)

Can Ye, Chaoyang Xue, Pengfei Liu, Chenglong Zhang, Zhuobiao Ma, Yuanyuan Zhang, Chengtang Liu, Junfeng Liu, Keding Lu, Yujing Mu

### ► To cite this version:

Can Ye, Chaoyang Xue, Pengfei Liu, Chenglong Zhang, Zhuobiao Ma, et al.. Strong impacts of biomass burning, nitrogen fertilization, and fine particles on gas-phase hydrogen peroxide (H<sub>2</sub>O<sub>2</sub>). *Science of the Total Environment*, 2022, 843, pp.156997. 10.1016/j.scitotenv.2022.156997. insu-04046942

**HAL Id: insu-04046942**

**<https://insu.hal.science/insu-04046942v1>**

Submitted on 27 Sep 2024

**HAL** is a multi-disciplinary open access archive for the deposit and dissemination of scientific research documents, whether they are published or not. The documents may come from teaching and research institutions in France or abroad, or from public or private research centers.

L'archive ouverte pluridisciplinaire **HAL**, est destinée au dépôt et à la diffusion de documents scientifiques de niveau recherche, publiés ou non, émanant des établissements d'enseignement et de recherche français ou étrangers, des laboratoires publics ou privés.



Distributed under a Creative Commons Attribution 4.0 International License

# 1 Strong Impacts of Biomass Burning, Nitrogen Fertilization, and Fine 2 Particles on Gas-phase Hydrogen Peroxide (H<sub>2</sub>O<sub>2</sub>)

3 Can Ye<sup>1,2</sup>, Chaoyang Xue<sup>3\*</sup>, Pengfei Liu<sup>1,4,5</sup>, Chenglong Zhang<sup>1,4,5</sup>, Zhuobiao Ma<sup>1,4,5</sup>, Yuanyuan  
4 Zhang<sup>1,4,5</sup>, Chengtang Liu<sup>1,4,5</sup>, Junfeng Liu<sup>1,4,5</sup>, Keding Lu<sup>2</sup>, Yujing Mu<sup>1,4,5\*</sup>.

5 <sup>1</sup>Research Centre for Eco-Environmental Sciences, Chinese Academy of Sciences, Beijing 100085, China

6 <sup>2</sup>State Key Joint Laboratory of Environmental Simulation and Pollution Control, College of Environmental Sciences and  
7 Engineering, Peking University, Beijing 100871, China.

8 <sup>3</sup>Laboratoire de Physique et Chimie de l'Environnement et de l'Espace (LPC2E), CNRS – Université Orléans – CNES,  
9 45071 Orléans Cedex 2, France

10 <sup>4</sup>Centre for Excellence in Regional Atmospheric Environment, Institute of Urban Environment, Chinese Academy of  
11 Sciences, Xiamen 361021, China

12 <sup>5</sup>University of Chinese Academy of Sciences, Beijing 100049, China

13

14 *Correspondence to:* Chaoyang Xue (chaoyang.xue@cnrs-orleans.fr), Yujing Mu (yjmu@rcees.ac.cn)

15 **Abstract.** Gas-phase hydrogen peroxide (H<sub>2</sub>O<sub>2</sub>) plays an important role in atmospheric chemistry as an indicator of the  
16 atmospheric oxidizing capacity. It is also a vital oxidant of sulfur dioxide (SO<sub>2</sub>) in the aqueous phase, resulting in the  
17 formation of acid precipitation and sulfate aerosol. However, sources of H<sub>2</sub>O<sub>2</sub> are not fully understood especially in  
18 polluted areas affected by human activities. In this study, we reported some high H<sub>2</sub>O<sub>2</sub> cases observed during one  
19 summer and two winter campaigns conducted at a polluted rural site in the North China Plain. Our results showed that  
20 agricultural fires led to high H<sub>2</sub>O<sub>2</sub> concentrations up to 9 ppb, indicating biomass burning events contributed  
21 substantially to primary H<sub>2</sub>O<sub>2</sub> emission. In addition, elevated H<sub>2</sub>O<sub>2</sub> and O<sub>3</sub> concentrations were measured after

22 fertilization as a consequence of the enhanced atmospheric oxidizing capacity by soil HONO emission. Furthermore,  
23 H<sub>2</sub>O<sub>2</sub> exhibited unexpectedly high concentration under high NO<sub>x</sub> conditions in winter, which are closely related to  
24 multiphase reactions in particles involving organic chromophores. Our findings suggest that these special factors  
25 (biomass burning, fertilization, and ambient particles), which are not well considered in current models, are significant  
26 contributors to H<sub>2</sub>O<sub>2</sub> production, thereby affecting the regional atmospheric oxidizing capacity and the global sulfate  
27 aerosol formation.

28  
29 Key words: H<sub>2</sub>O<sub>2</sub>, biomass burning, fertilization, particles, organic chromophores

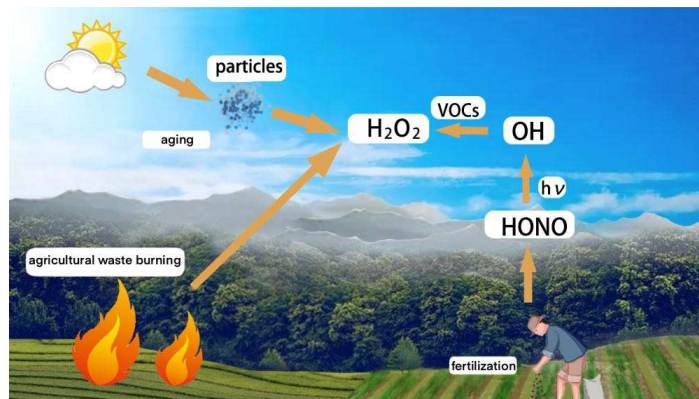
30

### 31 Highlights

- 32 ● Biomass burning events led to high H<sub>2</sub>O<sub>2</sub> concentrations up to 9 ppb observed.
- 33 ● H<sub>2</sub>O<sub>2</sub> and O<sub>3</sub> were greatly enhanced after fertilization events due to HONO emission by fertilized soil.
- 34 ● Particle-phase reactions involving organic chromophores contributed to H<sub>2</sub>O<sub>2</sub> production.

### 35 Graphical abstract

36



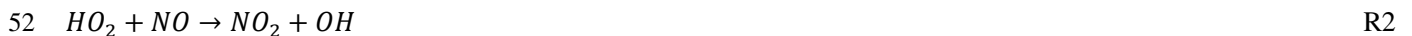
37

## 38 1 Introduction

39 Atmospheric hydrogen peroxide ( $H_2O_2$ ) acts as a temporary reservoir of  $HO_x$  ( $OH+HO_2$ ) radicals and hence an  
40 indicator of the oxidizing capacity of the atmosphere. Besides,  $H_2O_2$  itself is one of the most important oxidants in the  
41 atmosphere and can oxidize  $SO_2$  in clouds, droplets, and deliquesced particles (Penkett et al., 1979; Calvert and  
42 Stockwell, 1983), with the formation of sulfate, an important component of fine particulate matter that impacts air  
43 quality, climate, and human health (Grantz et al., 2003; Nel, 2005; Fuzzi et al., 2015). Furthermore,  $H_2O_2/HNO_3$  was  
44 suggested as a robust indicator to determine whether ozone production is more sensitive to  $NO_x$  or VOCs (Sillman,  
45 1995; Sillman et al., 1998). Vermeuel et al. (2019) evaluated the sensitivity of  $O_3$  to VOCs and  $NO_x$  alongside the  
46 Lake Michigan Coastline utilizing the modeled ratio of  $H_2O_2$  and  $HNO_3$  production rates. Results indicated that the  $O_3$   
47 production was strongly VOC-limited in the urban areas and became more  $NO_x$ -limited as the plume advected North.  
48 As  $O_3$  pollution is becoming a big concern with increase of  $NO_x$  and VOCs emissions (Tan et al., 2018; Yu et al.,  
49 2020),  $H_2O_2$  has drawn more attention in both urban and rural areas.



51  $k_{R1}=1.5\times 10^{-12} \text{ cm}^3 \text{ molecule}^{-1} \text{ s}^{-1}$  at 298 K



53  $k_{R2}=8.9\times 10^{-12} \text{ cm}^3 \text{ molecule}^{-1} \text{ s}^{-1}$  at 298 K

54 Based on the current understanding,  $H_2O_2$  is mainly produced by the self-reaction of two hydroperoxy radicals ( $HO_2$ )  
55 (R1), which are produced from the oxidation of hydrocarbons by  $OH$  radicals or the photolysis of formaldehyde. R1  
56 largely depends on ambient  $NO_x$  levels. With high  $NO_x$  levels, R2 would dominate relative to R1 due to more rapid  
57  $HO_2$  consumption through R2. For example, with typical noontime  $NO$  concentration of 1 ppb and  $HO_2$  concentration  
58 of  $4\times 10^7 \text{ molecules cm}^{-3}$  observed or modelled in the winter NCP (Ma et al., 2019; Slater et al., 2020; Xue et al., 2020),  
59  $HO_2$  loss rate through R2 ( $8.4\times 10^6 \text{ molecules cm}^{-3} \text{ s}^{-1}$ ) is 3 orders of magnitude faster than that of R1 ( $2.6\times 10^3$   
60  $\text{molecules cm}^{-3} \text{ s}^{-1}$ ). Field measurements also supported that under the condition of  $NO$  concentrations exceeding 1

61 ppb, H<sub>2</sub>O<sub>2</sub> production through R1 will be substantially suppressed (Walker et al., 2006; He et al., 2010; Watanabe et  
62 al., 2018). Besides the H<sub>2</sub>O<sub>2</sub> formation channel through R1, ozonolysis of alkenes also contributes to H<sub>2</sub>O<sub>2</sub> production,  
63 which could proceed without sunlight (Becker et al., 1990; Hua et al., 2008). The main sinks of H<sub>2</sub>O<sub>2</sub> include  
64 photolysis, dry deposition, reaction with OH radicals, and reaction with SO<sub>2</sub> in the liquid phase. The typical photolysis  
65 rate of H<sub>2</sub>O<sub>2</sub> daily maximum value is  $6.0 \times 10^{-6} \text{ s}^{-1}$  in the northern midlatitude (Stockwell et al., 1997), corresponding to  
66  $\tau_{\text{photo}}=46 \text{ h}$  (lifetime against photolysis). As for the reaction of H<sub>2</sub>O<sub>2</sub> with OH radicals, the rate constant is  $1.7 \times 10^{-12}$   
67  $\text{cm}^3 \text{ molecule}^{-1} \text{ s}^{-1}$  at 298 K (Atkinson et al., 2004), and the temperature influence on the rate constant is small.  $\tau_{\text{H}_2\text{O}_2}$   
68 (lifetime with respect to OH reaction) is estimated to be around 32 h if OH concentration is assumed to be  $5 \times 10^6$   
69  $\text{molecule cm}^{-3}$ . Assuming the dry deposition velocity of H<sub>2</sub>O<sub>2</sub> is about  $2 \text{ cm s}^{-1}$  (Liang et al., 2013), the lifetime of  
70 H<sub>2</sub>O<sub>2</sub> with respect to dry deposition is 7 h with a boundary height of 1 km. Therefore, dry deposition loss was a  
71 dominant factor influencing the lifetime of H<sub>2</sub>O<sub>2</sub> in the atmosphere.

72 H<sub>2</sub>O<sub>2</sub> formation does not only depend on NO<sub>x</sub> levels, which was discussed earlier but also as a function of many other  
73 chemical and physical parameters. First of all, H<sub>2</sub>O<sub>2</sub> concentrations are affected by precursors concentrations like  
74 VOCs. High VOC to NO<sub>x</sub> ratio leads to more HO<sub>2</sub> production, in favor of the production of H<sub>2</sub>O<sub>2</sub> (Lee et al., 2008;  
75 Crowley et al., 2018). O<sub>3</sub> and HONO, which are important contributors to OH radicals in the lower troposphere, also  
76 have crucial effect on H<sub>2</sub>O<sub>2</sub> formation under certain atmospheric conditions. For instance, in a clean environment, OH  
77 radicals mainly come from O<sub>3</sub> photolysis followed by the reaction of O(<sup>1</sup>D) with water vapor. In polluted areas (like  
78 urban sites), HONO appeared to be an important source of OH radicals (Elshorbany et al., 2010; Xue et al., 2020). In  
79 addition, since H<sub>2</sub>O<sub>2</sub> is very soluble with high Henry's law constant of  $1.07 \times 10^5 \text{ M atm}^{-1}$  at 298 K (Lee et al., 2000;  
80 Reeves and Penkett, 2003), H<sub>2</sub>O<sub>2</sub> can be readily consumed via reaction with SO<sub>2</sub> in the atmospheric aqueous phase  
81 (Penkett et al., 1979; Hoffmann and Edwards, 1975). Hence, high SO<sub>2</sub> concentrations are usually associated with low  
82 H<sub>2</sub>O<sub>2</sub> concentrations (Watanabe et al., 2016; Guo et al., 2014). Moreover, solar radiation has a significant impact on  
83 H<sub>2</sub>O<sub>2</sub> concentrations. Model simulations by Kleinman et al. showed that a 60% decrease in solar radiation intensity  
84 could lead to a 65% decrease in H<sub>2</sub>O<sub>2</sub> concentrations (Kleinman, 1986), which highlights the important role of solar

85 radiation in the formation of H<sub>2</sub>O<sub>2</sub>. The absolute humidity is an important factor for H<sub>2</sub>O<sub>2</sub> formation as high humidity  
86 may lead to an increase in OH radical and hence more H<sub>2</sub>O<sub>2</sub> production (Hamilton Jr and Lii, 1977; Fischer et al.,  
87 2019). Also, higher temperature promotes the rate of photochemical reactions, resulting in more radical production and  
88 hence more H<sub>2</sub>O<sub>2</sub> production (Das and Aneja, 1994; Nunnermacker et al., 2008; Zhang et al., 2018). These factors are  
89 well understood and all considered in the box model and regional transport models. However, it was reported that  
90 H<sub>2</sub>O<sub>2</sub> was still underestimated during polluted periods, indicating that some extra factors affecting H<sub>2</sub>O<sub>2</sub> concentrations  
91 may be neglected (Qin et al., 2018; Ye et al., 2018). Moreover, there is still a gap between modeled and measured  
92 sulfate concentrations during haze events, suggesting sulfate formation is not completed in current mechanisms (Wang  
93 et al., 2014; Zheng et al., 2015). Hence, it is essential to incorporate all processes related to H<sub>2</sub>O<sub>2</sub> formation into  
94 regional models for better predictions. However, there is a relatively small body of literature that is concerned with  
95 gas-phase H<sub>2</sub>O<sub>2</sub> measurements in China (Wang et al., 2016; Qin et al., 2018; Ye et al., 2018; Zhang et al., 2018),  
96 especially in the North China Plain (NCP) where it is encountering serious air pollution.

97 In order to more accurately predict H<sub>2</sub>O<sub>2</sub> concentrations and evaluate its role in the oxidizing capacity of the  
98 atmosphere, a comprehensive investigation of factors controlling gaseous H<sub>2</sub>O<sub>2</sub> should be conducted. In this study,  
99 H<sub>2</sub>O<sub>2</sub> and other relevant pollutants were simultaneously measured at a polluted rural site in the NCP in summertime  
100 (31 May to 8 July 2017) and wintertime (1 November to 31 December 2017, 1 to 15 December 2018). Time series of  
101 H<sub>2</sub>O<sub>2</sub> and related parameters in the three field campaigns were shown in Figure S1. In addition to the factors mentioned  
102 above, some special factors were also found to profoundly affect atmospheric H<sub>2</sub>O<sub>2</sub> concentrations in our study, which  
103 might be overlooked by the current understanding. The following will be some cases observed in our field  
104 measurements to reveal these special factors.

## 105 **2 Experiments**

### 106 **2.1 Measurement site**

107 The measurements were conducted at a rural site (SRE-CAS, 38.66°N, 115.25°E) located in Wangdu County (Liu et  
108 al., 2017; Xue et al., 2020), in Hebei province, which is 150 km southwest of Beijing city in the NCP. This site was  
109 surrounded by vast areas of farmlands and impacted by coal combustion in winter and agricultural activities such as  
110 biomass burning and fertilization in summer. A high-speed way was located 2 km southwest of the site. There are no  
111 industries around the sampling site. All instruments were placed into a container with the sampling inlet about 3.4 m  
112 above the ground.

### 113 **2.2 Measurement methods**

114 A Germany commercial H<sub>2</sub>O<sub>2</sub> monitor (AEROLASER AL-2021) based on a wet chemical technique was employed to  
115 measure gas-phase H<sub>2</sub>O<sub>2</sub>. Firstly, soluble peroxides, including H<sub>2</sub>O<sub>2</sub> and organic peroxides, were sampled by a  
116 stripping coil with a buffered solution. In order to distinguish H<sub>2</sub>O<sub>2</sub> and organic peroxides, the stripping solution was  
117 divided into two channels. In the first channel, the peroxides in the stripping solution react with p-hydroxyphenyl  
118 acetic acid (POPHA) under the catalysis of peroxidase, resulting in the formation of fluorescent dye. After excitation at  
119 326 nm, the fluorescence could be detected at 400-420 nm. In the second channel, before peroxides reaction with  
120 POPHA, enzyme catalase was added to selectively destroy H<sub>2</sub>O<sub>2</sub>. Then H<sub>2</sub>O<sub>2</sub> was determined as the difference between  
121 the two channels. Liquid calibration was performed every two days. The detection limit of the instrument was <50 ppt.  
122 Detailed information can be found in our previous study (Ye et al., 2018).

123 HONO was measured by a commercial long path absorption photometer instrument (LOPAP, Model-03, QUMA)  
124 (Heland et al., 2001). Briefly, ambient air was sampled by using two same stripping coils connected in series. Because  
125 HONO is highly soluble, almost all the ambient HONO was absorbed by the absorption solution in the first stripping  
126 coil, while possibly interfering species were sampled in the first as well as the second stripping coil. Thus, the signal

127 difference between the two channels can largely eliminate the possible influence of the interfering species on the  
128 HONO measurement. Instrument background was conducted by sampling ultrapure nitrogen twice per day. The  
129 instrument has a detection limit of <5 ppt on 5 min average.

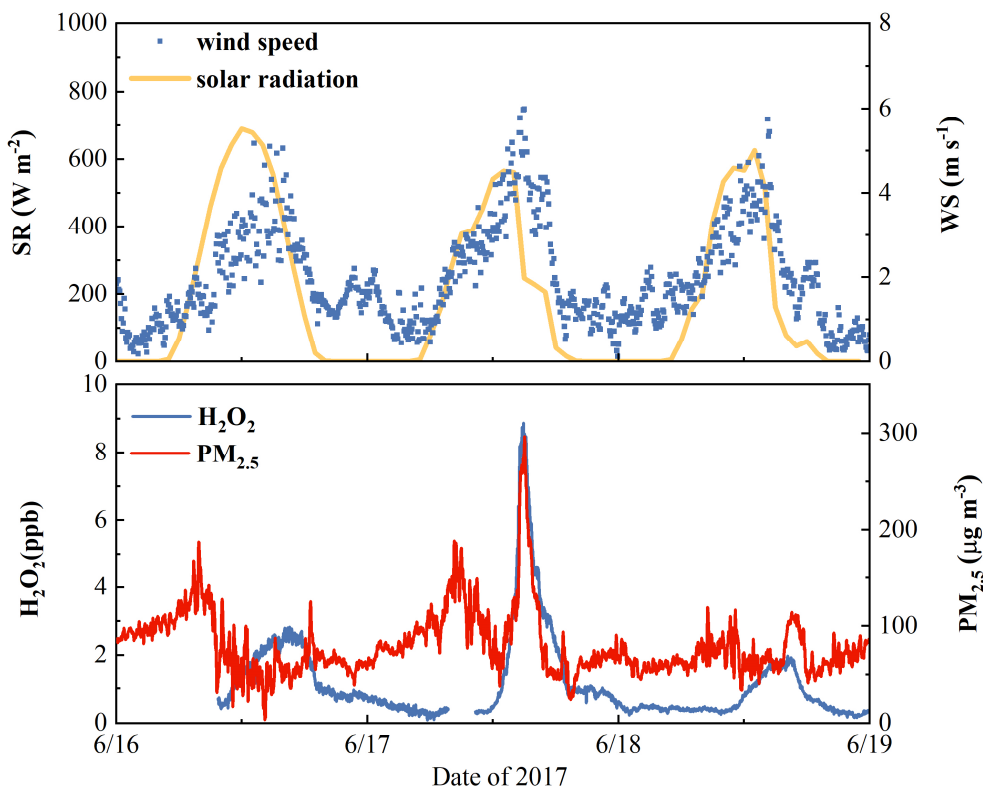
130 NO and NO<sub>2</sub> were measured with a chemiluminescence analyzer (Thermo Environmental Instruments (TEI), Model  
131 42i) equipped with a photolytic converter. Ozone (O<sub>3</sub>) was measured by a commercial UV photometric analyzer (TEI  
132 Model 49i). SO<sub>2</sub> was measured by a pulsed fluorescence SO<sub>2</sub> analyzer (Model 43i). The analyzers of NO<sub>x</sub> (NO/NO<sub>2</sub>),  
133 O<sub>3</sub> and SO<sub>2</sub> were regularly calibrated once per week. PM<sub>2.5</sub> levels were measured by a standard Tapered Element  
134 Oscillating Microbalance system (TEOM 1400A, Thermo Scientific). Organic carbon (OC) and elemental carbon (EC)  
135 were measured by using an online organic/elemental carbon analyzer (TR20N9, CECEP Talroad Technology Co.,  
136 Ltd., China). Meteorological measurements (temperature, pressure, wind speed and direction, relative humidity, and  
137 solar radiation) were achieved by a portable weather station (Model WXT520, Vaisala, Finland).

### 138 **3 Results and discussion**

#### 139 **3.1 Influence of biomass burning events on H<sub>2</sub>O<sub>2</sub> chemistry**

140 Figure 1 depicts the time series of H<sub>2</sub>O<sub>2</sub>, PM<sub>2.5</sub>, and some meteorological parameters from 16 to 19 June 2017. H<sub>2</sub>O<sub>2</sub>  
141 exhibited a typical diurnal pattern with a maximum in the early afternoon and low concentrations during the night and  
142 in the morning. For instance, on 16 June, H<sub>2</sub>O<sub>2</sub> reached a maximum value of ~2.5 ppb around 15:00 LST (Local  
143 Standard Time). However, at 13:00 LST on the following day, H<sub>2</sub>O<sub>2</sub> increased remarkably from ~1 to ~9 ppb in two  
144 hours. Notably, PM<sub>2.5</sub> also increased concurrently with H<sub>2</sub>O<sub>2</sub> from ~50 to ~300 μg m<sup>-3</sup>.



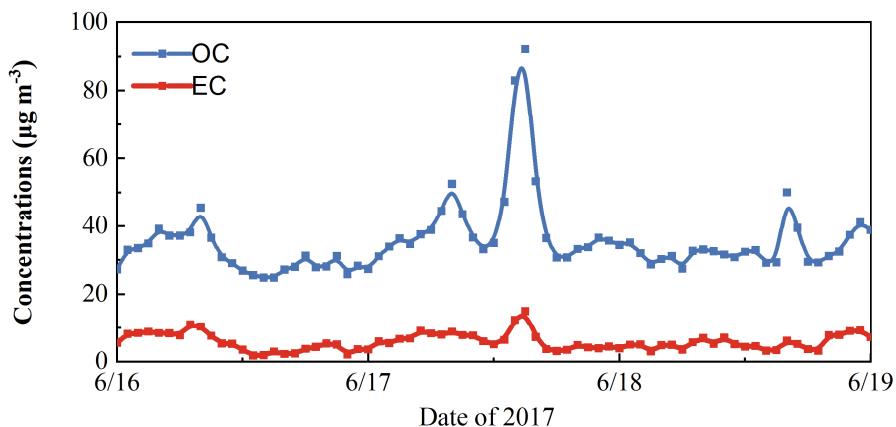


145

146 **Figure 1: Time series of H<sub>2</sub>O<sub>2</sub>, PM<sub>2.5</sub>, solar radiation, and wind speed from 16 to 19 June 2017 in the summer**  
 147 **campaign. H<sub>2</sub>O<sub>2</sub> and PM<sub>2.5</sub> were shown in minute-average data.**

148 The significantly positive correlation between H<sub>2</sub>O<sub>2</sub> and PM<sub>2.5</sub> from 13:00 to 18:00 during the event ( $r^2=0.97$ )  
 149 indicated the same reason for their increases. However, the wind speed was high during the elevation period (~4-6 m s  
 150 <sup>-1</sup>), and there wasn't a significant difference in the solar radiation with regard to other days, indicating photochemical  
 151 reactions alone couldn't explain the sharp increase of H<sub>2</sub>O<sub>2</sub> in such a short period. Considering the high wind speed  
 152 when the high H<sub>2</sub>O<sub>2</sub> event was observed, the exceptionally high H<sub>2</sub>O<sub>2</sub> might be ascribed to the regional transport of  
 153 H<sub>2</sub>O<sub>2</sub> from the emission source. In addition, the OC (organic carbon) to EC (elemental carbon) ratio at 15:00 LST  
 154 being higher than 5 (Figure 2) suggested a biomass burning event encountered here (Watson et al., 2001). The well-  
 155 defined shape and narrow width of the observed H<sub>2</sub>O<sub>2</sub> within the plume indicated that the plume had not experienced

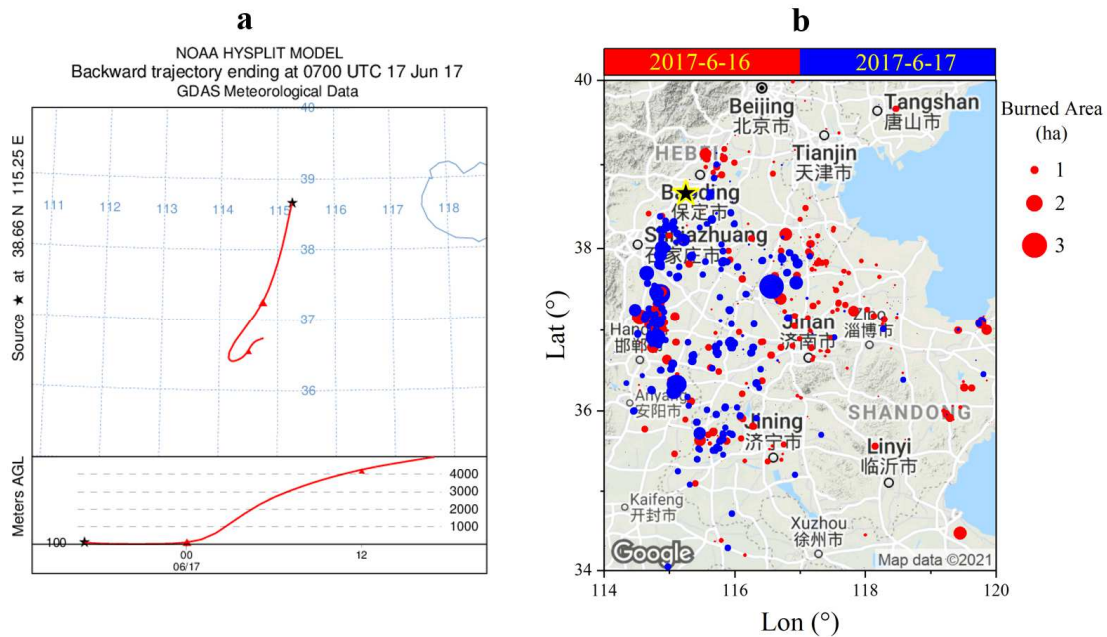
156 significant dispersion and mixing since it was emitted, suggesting that the sampling site is not far from the emission  
157 source.



158  
159 **Figure 2: Time series of OC and EC from 16 to 19 June 2017 in the summer campaign.**

160 Given the short lifetime of H<sub>2</sub>O<sub>2</sub> in the atmosphere (typically less than one day), we calculated 1-day back trajectory  
161 with the HYSPLIT model (<https://www.ready.noaa.gov/HYSPLIT.php>, last access: 15 April 2022) and found the  
162 sampling site was influenced by the plume coming from the southern areas (Figure 3a). The fire spot data on 16 June  
163 and 17 June showed that south areas were filled with dense fire spots (Figure 3b), indicative of large areas of  
164 agricultural (wheat straw) fires. Large areas of biomass burning in farmland contributed to the primary H<sub>2</sub>O<sub>2</sub> emission,  
165 resulting in the high H<sub>2</sub>O<sub>2</sub> concentrations measured at the downwind site. Lee et al. (1997) observed H<sub>2</sub>O<sub>2</sub>  
166 concentrations up to 10 ppb and attributed this to the direct production of H<sub>2</sub>O<sub>2</sub> within biomass burning plumes. Some  
167 studies also found an underestimation of modelled H<sub>2</sub>O<sub>2</sub> concentration compared with observations during biomass  
168 burning events (Wang et al., 2016; Crowley et al., 2018). H<sub>2</sub>O<sub>2</sub> concentrations at our sampling site increased by a  
169 factor of ~5 (from ~2 ppb to ~9 ppb), which is larger than the value (1.2-3.6) observed in biomass burning plumes by a  
170 recent study (Allen et al., 2022). The difference may be explained by the different photochemical age of the air mass  
171 sampled. In addition to primary emission, H<sub>2</sub>O<sub>2</sub> concentrations will also increase with the photoaging of the biomass  
172 burning plume as a consequence of abundant precursors contributing to secondary H<sub>2</sub>O<sub>2</sub> production (Yokelson et al.,  
173 2009). Moreover, low NO<sub>x</sub> levels at the rural areas are conducive for secondary H<sub>2</sub>O<sub>2</sub> production. Unfortunately, we

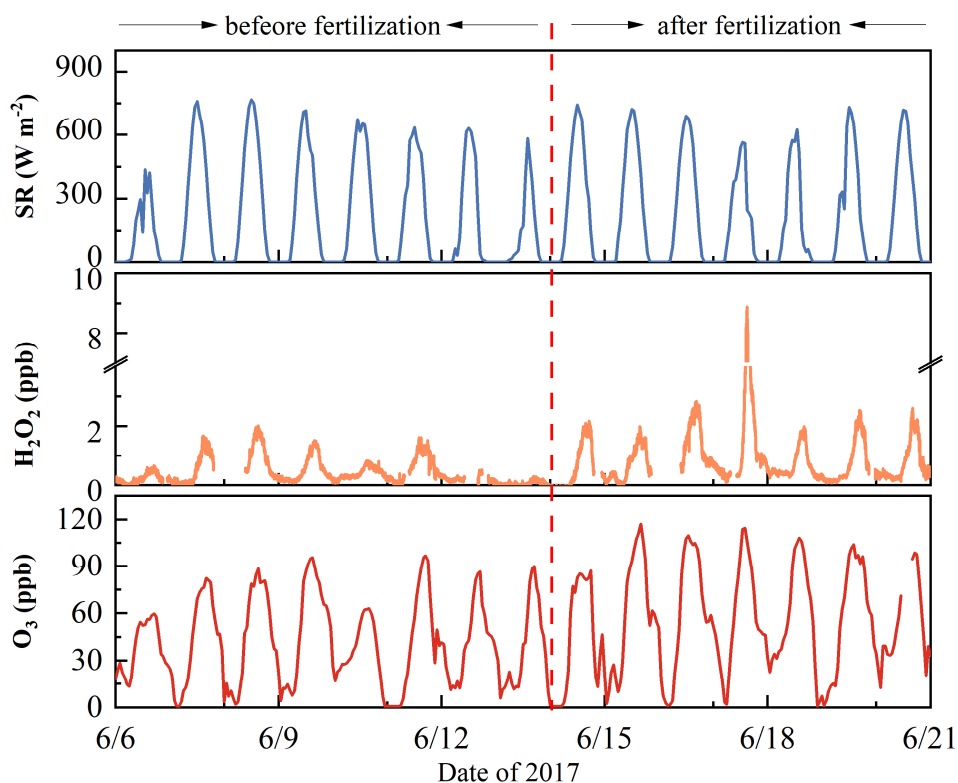
174 are unable to distinguish primary emission from secondary production during the plume transport. Our results provided  
 175 direct field evidence that biomass burning events significantly affect H<sub>2</sub>O<sub>2</sub> concentrations, despite the polluted plume  
 176 was already aged or diluted. The primary and secondary H<sub>2</sub>O<sub>2</sub> produced from biomass burning contributes to odd-  
 177 hydrogen radicals, thereby affecting the oxidizing capacity of the atmosphere. Given that wildfire is increasing  
 178 globally and agricultural fires can be commonly seen during harvesting seasons worldwide (Andreae et al., 2019; Liu  
 179 et al., 2015), they are expected to make great contributions to H<sub>2</sub>O<sub>2</sub> production. To better evaluate the global  
 180 consequence of the biomass burning-related H<sub>2</sub>O<sub>2</sub> production, the emission factor and the production mechanism need  
 181 to be critically determined.



182  
 183 **Figure 3. (a) 24 h-trajectory arriving at SRE-CAS site at 15:00 (UTC+8), 17 July 2017 when the peak H<sub>2</sub>O<sub>2</sub>**  
 184 **occurred. (b) Fire spots map on 16 and 17 June 2017 UTC time obtained from the FINN biomass burning**  
 185 **inventory (Wiedinmyer et al., 2011). The sampling site is represented by a black triangle. Map copyright:**  
 186 **GoogleMap.**

187 **3.2 Influence of nitrogen fertilization on the H<sub>2</sub>O<sub>2</sub> chemistry**

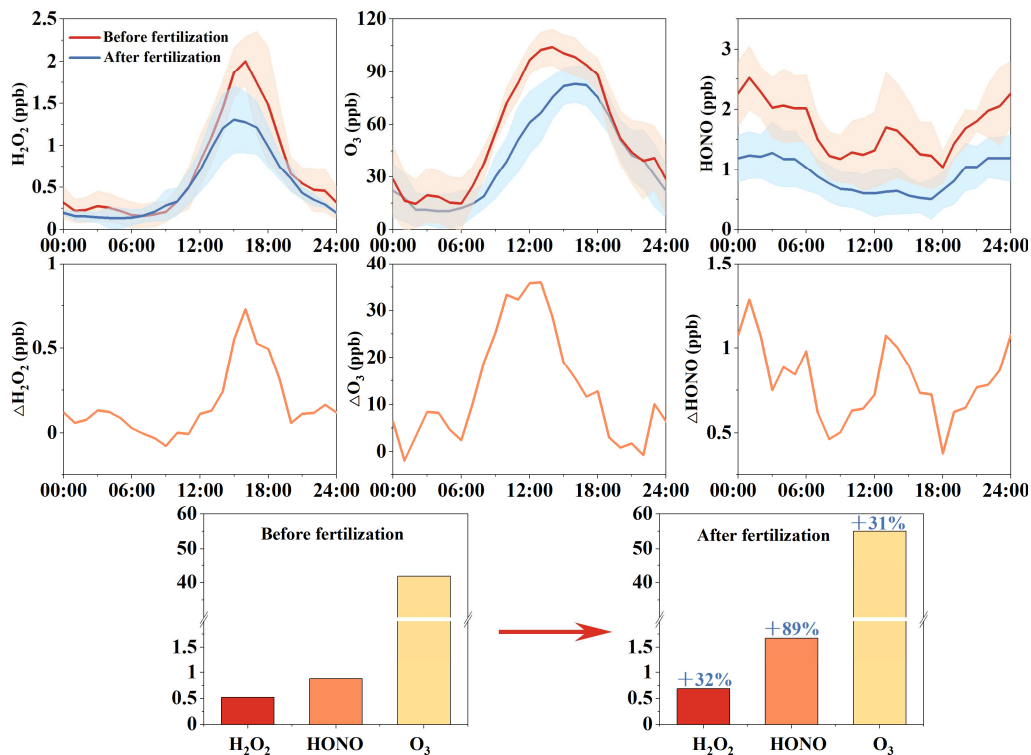
188 The summer campaign covered the important agricultural activities period like fertilization. The fertilization process  
189 for the agricultural fields around our station was conducted on 13 June, 2017. Details about the fertilization event can  
190 be found in our recent study, in which HONO emissions from the fertilized fields were discussed and its potential  
191 impacts on O<sub>3</sub> and H<sub>2</sub>O<sub>2</sub> were preliminarily mentioned (Xue et al., 2021). Figure 4 exhibited the time series of H<sub>2</sub>O<sub>2</sub>,  
192 O<sub>3</sub> and solar radiation before (6-14 June) and after (14-21 June) the fertilization event. H<sub>2</sub>O<sub>2</sub> and O<sub>3</sub> showed  
193 pronounced diurnal patterns that were similar to those observed for solar radiation. After fertilization, both H<sub>2</sub>O<sub>2</sub> and  
194 O<sub>3</sub> diurnal peak values evidently increased (Figure 4 and Figure 5).



195

196 **Figure 4: Time series of H<sub>2</sub>O<sub>2</sub>, O<sub>3</sub> and solar radiation intensity before (6-14 June) and after (14-21 June) the**  
197 **fertilization. The red line indicates the time when the fertilization event around the site began.**

198 To more accurately elaborate on the influence of fertilization events on H<sub>2</sub>O<sub>2</sub>, the H<sub>2</sub>O<sub>2</sub> concentrations on 17 June,  
199 which were mainly affected by biomass burning events as discussed in Section 3.1, were not taken into consideration.  
200 The averaged concentrations of H<sub>2</sub>O<sub>2</sub> and O<sub>3</sub> were a factor of 1.32 and 1.31 higher than the levels observed before the  
201 fertilization events (Figure 5), but the solar radiation didn't show a significant change, indicating that fertilization may  
202 promote the formation of H<sub>2</sub>O<sub>2</sub> and O<sub>3</sub>. Previous laboratory studies have reported that fertilized soil could be a source  
203 of HONO with the use of nitrogen fertilizer (Su et al., 2011; Donaldson et al., 2014). Our previous work also provided  
204 field evidence for soil HONO emission after fertilization at this site (Xue et al., 2019). Therefore, one can expect that  
205 HONO concentrations may increase after the fertilization and subsequent HONO photolysis could release more OH  
206 radicals compared to the period before fertilization, thereby accelerating the photochemical production of H<sub>2</sub>O<sub>2</sub> and  
207 O<sub>3</sub>. Further analysis confirmed that after fertilization events the enhancements of H<sub>2</sub>O<sub>2</sub> and O<sub>3</sub> were consistent with the  
208 rising ambient HONO levels (Figure 5). Additionally, the significant increase in H<sub>2</sub>O<sub>2</sub> ( $\Delta$ H<sub>2</sub>O<sub>2</sub>) and O<sub>3</sub> ( $\Delta$ O<sub>3</sub>) appeared  
209 around noontime, coincident with the HONO enhancement ( $\Delta$ HONO) (Figure 5) and inferred soil HONO emission  
210 flux in Xue et al. (2021). It is worth mentioning that Tan et al. (2017) reported high OH concentrations up to  $3 \times 10^7$   
211 cm<sup>-3</sup> at the same rural site during a summer campaign in 2014, which was ascribed to local HONO emission from the  
212 fertilized agricultural fields (Liu et al., 2019). Therefore, agricultural activities may strongly influence the atmospheric  
213 oxidizing capacity and hence the concentrations of H<sub>2</sub>O<sub>2</sub>, which should be better constrained in atmospheric chemical  
214 transport models to assess the impacts of H<sub>2</sub>O<sub>2</sub> on regional air quality and global climate.

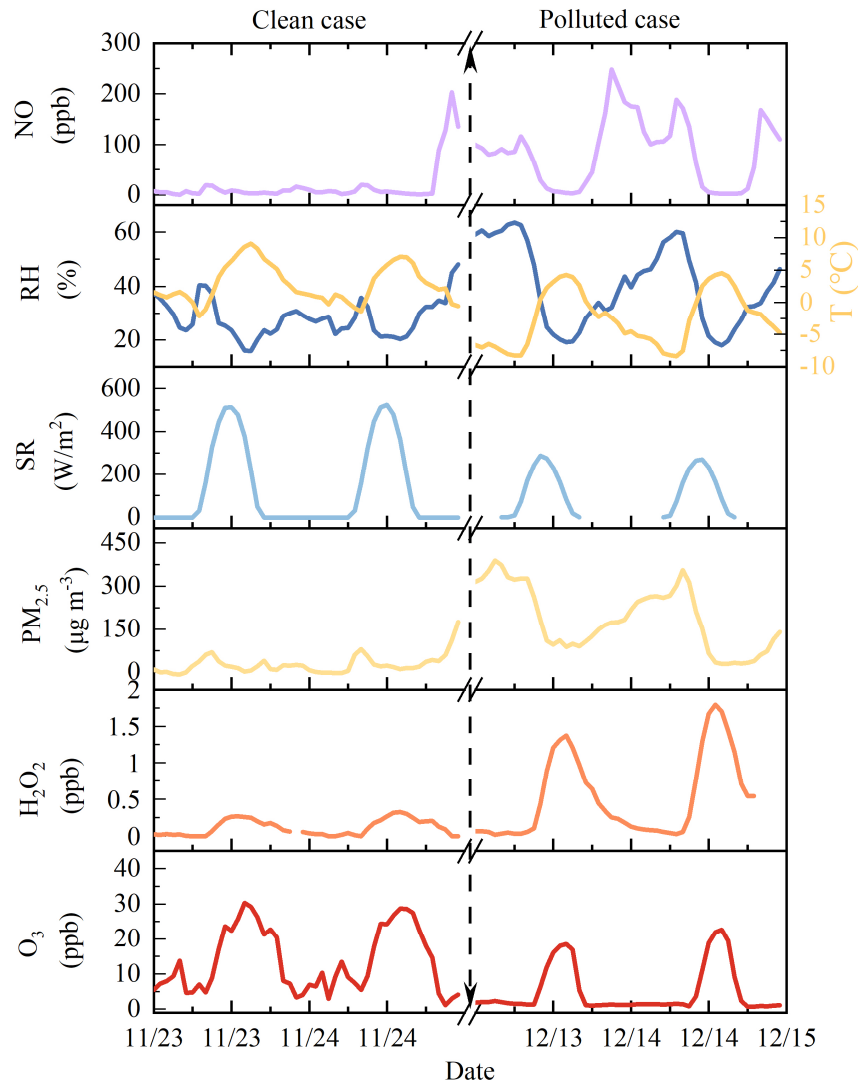


215

216 **Figure 5: Average concentrations of H<sub>2</sub>O<sub>2</sub>, HONO and O<sub>3</sub> before (6-14 June) and after (14-21 June) the**  
 217 **fertilization in June 2017.**

218 **3.3 Influence of particles on H<sub>2</sub>O<sub>2</sub> chemistry**

219 To investigate H<sub>2</sub>O<sub>2</sub> production on clean and polluted days in the wintertime, representative cases were selected based  
 220 on PM<sub>2.5</sub> levels. Figure 6 shows H<sub>2</sub>O<sub>2</sub> and other related chemical species and meteorological parameters measured  
 221 during the winter campaign. In winter, the photochemical generation of OH radicals is weak as a consequence of  
 222 significantly reduced solar radiation intensity, water vapor and ozone concentrations. Thus, the concentrations of  
 223 secondary oxidants like H<sub>2</sub>O<sub>2</sub> levels are typically believed to be low (Xue et al., 2016). On 23 and 24 November 2017  
 224 during our field measurements (the clean case in Figure 6), the maximum solar radiation intensity was lower than 500  
 225 W m<sup>-2</sup> and O<sub>3</sub> concentrations were less than 30 ppb, indicative of the low photochemical activity compared to summer  
 226 seasons. The corresponding observed H<sub>2</sub>O<sub>2</sub> concentrations were less than 0.35 ppb in the clean case.



227

228 **Figure 6: H<sub>2</sub>O<sub>2</sub>, NO, PM<sub>2.5</sub>, O<sub>3</sub>, solar radiation intensity (Sa), relative humidity (RH) and temperature (T)**  
 229 **measured in winter. Left panel: clean case (daily-averaged PM<sub>2.5</sub> concentrations lower than 75 µg m<sup>-3</sup>) from 23**  
 230 **to 25 November 2017; Right panel: polluted case (daily-averaged PM<sub>2.5</sub> concentrations higher than 75 µg m<sup>-3</sup>)**  
 231 **from 13 to 15 December 2018.**

232 In contrast, during the polluted case, the maximum solar radiation intensity (~300 W m<sup>-2</sup>) and O<sub>3</sub> concentrations (~25  
 233 ppb) were lower than that in the clean case, while the maximum H<sub>2</sub>O<sub>2</sub> concentrations (> 1.5 ppb) in the polluted case

234 (Figure 6) were four times higher than that in the clean case. Contrary to our conventional thought, measured H<sub>2</sub>O<sub>2</sub>  
 235 concentrations during the polluted periods were unexpectedly high, which were even similar to summer levels.  
 236 It should be noted that the periods when H<sub>2</sub>O<sub>2</sub> grew rapidly coincided with high NO levels exceeding several tens ppb  
 237 (Figure 6). As discussed in the introduction section, the reaction rate of R2 was more than three orders of magnitude  
 238 higher than R1 under the condition of 1 ppb NO. Therefore, gas-phase recombination of HO<sub>2</sub> radicals couldn't explain  
 239 the high H<sub>2</sub>O<sub>2</sub> levels observed. The peak value of H<sub>2</sub>O<sub>2</sub> average diurnal pattern during polluted days (daily-averaged  
 240 PM<sub>2.5</sub>> 75 μg m<sup>-3</sup>) was evidently higher than that during clean days (daily-averaged PM<sub>2.5</sub>< 75 μg m<sup>-3</sup>), indicating  
 241 particles promoting H<sub>2</sub>O<sub>2</sub> production (Figure S2). Moreover, H<sub>2</sub>O<sub>2</sub> exhibited a pronounced diurnal pattern following  
 242 the track of solar radiation, which implied that H<sub>2</sub>O<sub>2</sub> was possibly photochemically produced. Taking all these hints  
 243 into account, in-particle photochemical reactions are likely to produce the gas-phase H<sub>2</sub>O<sub>2</sub>. Some other typical cases  
 244 (two clean and two polluted cases) were also identified and summarized in Table 1. These polluted cases with high  
 245 H<sub>2</sub>O<sub>2</sub> levels were observed in different years and should therefore be representative to reveal the promotion effect of  
 246 particles on H<sub>2</sub>O<sub>2</sub> production.

247 **Table 1. Summary of the clean and polluted cases**

Case type	Date	Average PM <sub>2.5</sub> (μg m <sup>-3</sup> )	H <sub>2</sub> O <sub>2</sub> maximum increase rate <sup>a</sup> (ppb h <sup>-1</sup> )	Maximum H <sub>2</sub> O <sub>2</sub> (ppb)
Clean	8 December 2017	14	0.05	0.36
	4 December 2018	32	0.04	0.21
Polluted	21 December 2017	135	0.266	1.16
	22 December 2017	216	0.267	1.19

248 <sup>a</sup>H<sub>2</sub>O<sub>2</sub> increase rate was calculated as (C<sub>t+1</sub>-C<sub>t</sub>)/1 h. C<sub>t</sub> represents the hourly-averaged H<sub>2</sub>O<sub>2</sub> concentrations at time t.

249

250 Previous studies have reported the photochemical production of H<sub>2</sub>O<sub>2</sub> free of NO suppression effect in the atmospheric  
 251 aqueous phase like in clouds and fog water (Faust et al., 1993; Anastasio et al., 1994; Zuo and Hoigné, 1993;  
 252 Anastasio et al., 1997). The observation is also consistent to our recent chamber and flow tube studies which revealed



253 that photochemical aging of particles involving organic chromophores could produce gas-phase  $\text{H}_2\text{O}_2$  (Ye et al., 2021;  
254 Liu et al., 2021). Organic chromophores have long been identified as important contributors to the aqueous photo-  
255 production of  $\text{H}_2\text{O}_2$  (Faust et al., 1993; Anastasio et al., 1997; Arellanes et al., 2006; Fang et al., 2019). The filter  
256 sample analysis showed that particles at our sampling site in winter contained a significant concentration of light-  
257 absorbing chromophores (Wang et al., 2020). Considering the photoactivity and abundance of organic chromophores  
258 in particles (Poschl and Shiraiwa, 2015; Herrmann et al., 2015), particles may have a crucial effect on the  
259 photochemical production of gas-phase  $\text{H}_2\text{O}_2$ . In winter, especially under the conditions of high NO presence, this  
260 multiphase reaction channel for  $\text{H}_2\text{O}_2$  formation, which is less sensitive to NO concentration, may play a more  
261 important role than the classical self-reaction of  $\text{HO}_2$  radicals, thereby contributing to more sulfate formation. The  
262 enhanced photochemical release of  $\text{H}_2\text{O}_2$  and subsequent oxidation of  $\text{SO}_2$  could also shed light on the discrepancy  
263 between observed and modeled sulfate concentrations during polluted periods.

264 A recent study found evident  $\text{O}_2^-$  and sulfate production on Beijing urban  $\text{PM}_{2.5}$  filter samples under simulated UV  
265 radiation (Zhang et al., 2020). This study also indicated that  $\text{H}_2\text{O}_2$  might be produced in the aging process of  $\text{PM}_{2.5}$  and  
266 subsequent  $\text{H}_2\text{O}_2$ -oxidation leads to the formation of sulfate, which is in agreement with our findings based on field  
267 measurements. Further work is needed to fully understand this unique  $\text{H}_2\text{O}_2$ -production pathway and assess its impacts  
268 on the global  $\text{H}_2\text{O}_2$  abundance and sulfate budget.

#### 269 **4 Conclusions and implications**

270 Several field campaigns with measurements on atmospheric  $\text{H}_2\text{O}_2$  and related parameters were conducted in the rural  
271 NCP during different seasons. It allows a determination of special factors (biomass burning, fertilization, and ambient  
272 particles) influencing gas-phase  $\text{H}_2\text{O}_2$  concentrations in this region. First, biomass burning plumes with high  $\text{H}_2\text{O}_2$   
273 concentrations up to 9 ppb were observed during a summer campaign. The measured  $\text{H}_2\text{O}_2$  rapidly increased from 1  
274 ppb to 9 ppb in two hours. Such a high  $\text{H}_2\text{O}_2$  level and rapid increase can't be solely explained by photochemical  
275 production. Along with the analysis of back-trajectory and fire spots data, high  $\text{H}_2\text{O}_2$  level was mainly attributed to

276 primary emission by large areas of biomass burning event. Second, a significant  $\text{H}_2\text{O}_2$  increase was observed after the  
277 agricultural nitrogen fertilization event in the summer. We found concurrent elevation of HONO levels compared to  
278 that before the fertilization events. The enhanced HONO levels, caused by the soil HONO emission from the fertilized  
279 agricultural fields, promoted the atmospheric oxidizing capacity and accelerated the production of secondary oxidants  
280 like  $\text{H}_2\text{O}_2$  and  $\text{O}_3$ . Third, high  $\text{H}_2\text{O}_2$  concentrations exceeding 1.5 ppb, were observed under the presence of several  
281 tens ppb NO during pollution episodes in the winter campaigns. Under such high NO conditions, the traditional gas-  
282 phase channel for  $\text{H}_2\text{O}_2$  formation would be greatly suppressed so that it was far to explained the measured  $\text{H}_2\text{O}_2$ . High  
283  $\text{H}_2\text{O}_2$  cases were typically accompanied by high  $\text{PM}_{2.5}$  levels, suggesting the potential role of particles in  $\text{H}_2\text{O}_2$   
284 production. Analogous to the aqueous  $\text{H}_2\text{O}_2$  production in the atmospheric aqueous phase like clouds by organic  
285 chromophores, high  $\text{H}_2\text{O}_2$  during winter polluted periods might be produced by chromophores in the particle phase  
286 considering the prevalence of chromophores in particles at this site.

287 Very limited measurements on atmospheric  $\text{H}_2\text{O}_2$  in China, especially in polluted regions, are currently available  
288 despite its important role in the atmospheric oxidizing capacity and sulfate aerosol formation. This study provides a  
289 unique dataset (one summer and two winter campaigns) of  $\text{H}_2\text{O}_2$  measurements in the NCP, which will benefit the  
290 assessment of model performance in the prediction of  $\text{H}_2\text{O}_2$  concentrations and its potential regional and global  
291 impacts. Our results also highlight the important roles of the special factors (biomass burning, fertilization, and  
292 ambient particles) in enhancing the concentrations of gas-phase  $\text{H}_2\text{O}_2$ . The enhanced  $\text{H}_2\text{O}_2$  production influenced by  
293 these special factors will contribute to the oxidizing capacity of the atmosphere and hence more sulfate aerosol  
294 formation, which has a crucial effect on air quality and direct forcing of the earth's climate. Additionally, particle-  
295 bound  $\text{H}_2\text{O}_2$  will further produce OH radical by photolysis and Fenton reaction, which will contribute to the aerosol  
296 aging and oxidizing organics within particles. Furthermore, reactive oxygen species (e.g.,  $\text{H}_2\text{O}_2$ , OH,  $\text{O}_2^-$ ) are at least  
297 partly responsible for the particle-related adverse health effect. The in-particle production of  $\text{H}_2\text{O}_2$  may constitute a  
298 public risk to human health. However, these special factors influencing  $\text{H}_2\text{O}_2$  concentrations are not well considered in  
299 model estimates of  $\text{H}_2\text{O}_2$  and may limit the accurate prediction of the  $\text{H}_2\text{O}_2$  budget in the atmosphere and its associated

300 climate and health effects. Hence, further research on the factors in controlling H<sub>2</sub>O<sub>2</sub> concentrations and model  
301 improvements in H<sub>2</sub>O<sub>2</sub> simulations are greatly warranted.

302

303 *Data availability.* Observation data are available at <https://zenodo.org/record/4456345#.YAp7DzMufX8>

304 *Competing interests.* The authors declare that they have no conflict of interest.

305 *Acknowledgements.* This work was supported by the National Natural Science Foundation of China (Nos. 41727805,  
306 41975164, 91544211, 22076202, 21976190, 41905109, 21876186), the China Postdoctoral Foundation  
307 (No.2021M700214), the PIVOTS project provided by the Region Centre -Val de Loire (ARD 2020 program and CPER  
308 2015 - 2020), and the Labex VOLTAIRE project (ANR-10-LABX-100-01). The authors thank Miss Wuqi Shen for the  
309 help with Graphical Abstract plotting.

## 310 **5 References**

311 Allen, H. M., Crouse, J. D., Kim, M. J., Teng, A. P., Ray, E. A., McKain, K., Sweeney, C., and Wennberg, P. O.: H<sub>2</sub>O<sub>2</sub>  
312 and CH<sub>3</sub>OOH (MHP) in the Remote Atmosphere: 1. Global Distribution and Regional Influences, *Journal of Geophysical*  
313 *Research: Atmospheres*, 127, e2021JD035701, <https://doi.org/10.1029/2021JD035701>, 2022.

314 Anastasio, C., Faust, B. C., and Allen, J. M.: Aqueous phase photochemical formation of hydrogen peroxide in authentic  
315 cloud waters, *Journal of Geophysical Research: Atmospheres*, 99, 8231-8248, 1994.

316 Anastasio, C., Faust, B. C., and Rao, C. J.: Aromatic carbonyl compounds as aqueous-phase photochemical sources of  
317 hydrogen peroxide in acidic sulfate aerosols, fogs, and clouds .1. Non-phenolic methoxybenzaldehydes and  
318 methoxyacetophenones with reductants (phenols), *Environ Sci Technol*, 31, 218-232, 1997.

319 Andreae, M. O.: Emission of trace gases and aerosols from biomass burning - an updated assessment, *Atmos Chem Phys*, 19,  
320 8523-8546, 2019.

321 Arellanes, C., Paulson, S. E., Fine, P. M., and Sioutas, C.: Exceeding of Henry's law by hydrogen peroxide associated with  
322 urban aerosols, *Environ Sci Technol*, 40, 4859-4866, 2006.

323 Atkinson, R., Baulch, D. L., Cox, R. A., Crowley, J. N., Hampson, R. F., Hynes, R. G., Jenkin, M. E., Rossi, M. J., and Troe,  
324 J.: Evaluated kinetic and photochemical data for atmospheric chemistry: Volume I - gas phase reactions of O-x, HOx,  
325 NOx and SOx species, *Atmos Chem Phys*, 4, 1461-1738, 2004.

326 Becker, K. H., Brockmann, K. J., and Bechara, J.: Production of hydrogen peroxide in forest air by reaction of ozone with  
327 terpenes, *Nature*, 346, 256-258, 1990.

328 Calvert, J. G., and Stockwell, W. R.: Acid generation in the troposphere by gas-phase chemistry, *Environ Sci Technol*, 17,  
329 428A-443A, 1983.

330 Crowley, J. N., Pouvesle, N., Phillips, G. J., Axinte, R., Fischer, H., Petäjä, T., Nölscher, A., Williams, J., Hens, K., and  
331 Harder, H.: Insights into HOx and ROx chemistry in the boreal forest via measurement of peroxyacetic acid, peroxyacetic  
332 nitric anhydride (PAN) and hydrogen peroxide, *Atmos Chem Phys*, 2018.

333 Das, M., and Aneja, V. P.: Analysis of Gaseous-Hydrogen Peroxide Concentrations in Raleigh, North-Carolina, *J Air Waste  
334 Manage*, 44, 176-180, 1994.

335 Donaldson, M. A., Bish, D. L., and Raff, J. D.: Soil surface acidity plays a determining role in the atmospheric-terrestrial  
336 exchange of nitrous acid, *P Natl Acad Sci USA*, 111, 18472-18477, 2014.

337 Elshorbany, Y. F., Kleffmann, J., Kurtenbach, R., Lissi, E., Rubio, M., Villena, G., Gramsch, E., Rickard, A. R., Pilling, M.  
338 J., and Wiesen, P.: Seasonal dependence of the oxidation capacity of the city of Santiago de Chile, *Atmos Environ*, 44,  
339 5383-5394, 2010.

340 Fang, T., Lakey, P. S. J., Weber, R. J., and Shiraiwa, M.: Oxidative Potential of Particulate Matter and Generation of  
341 Reactive Oxygen Species in Epithelial Lining Fluid, *Environ Sci Technol*, 53, 12784-12792, 2019.

342 Faust, B. C., Anastasio, C., Allen, J. M., and Arakaki, T.: Aqueous-phase photochemical formation of peroxides in authentic  
343 cloud and fog waters, *Science*, 260, 73-75, 1993.

344 Fischer, H., Axinte, R., Bozem, H., Crowley, J. N., Ernest, C., Gilge, S., Hafermann, S., Harder, H., Hens, K., and Janssen,  
345 R. H.: Diurnal variability, photochemical production and loss processes of hydrogen peroxide in the boundary layer over  
346 Europe, *Atmos Chem Phys*, 19, 11953-11968, 2019.

347 Fuzzi, S., Baltensperger, U., Carslaw, K., Decesari, S., van Der Gon, H. D., Facchini, M. C., Fowler, D., Koren, I., Langford,  
348 B., Lohmann, U., Nemitz, E., Pandis, S., Riipinen, I., Rudich, Y., Schaap, M., Slowik, J. G., Spracklen, D. V., Vignati, E.,  
349 Wild, M., Williams, M., and Gilardoni, S.: Particulate matter, air quality and climate: lessons learned and future needs,  
350 *Atmos Chem Phys*, 15, 8217-8299, 10.5194/acp-15-8217-2015, 2015.

351 Grantz, D. A., Garner, J. H. B., and Johnson, D. W.: Ecological effects of particulate matter, *Environ Int*, 29, 213-239, 2003.

352 Guo, J., Tilgner, A., Yeung, C., Wang, Z., Louie, P. K. K., Luk, C. W. Y., Xu, Z., Yuan, C., Gao, Y., Poon, S., Herrmann,  
353 H., Lee, S., Lam, K. S., and Wang, T.: Atmospheric Peroxides in a Polluted Subtropical Environment: Seasonal Variation,  
354 Sources and Sinks, and Importance of Heterogeneous Processes, *Environ Sci Technol*, 48, 1443-1450,  
355 10.1021/es403229x, 2014.

356 Hamilton Jr, E. J., and Lii, R. R.: The Dependence on H<sub>2</sub>O and on NH<sub>3</sub> of the Kinetics of the self-reaction of HO<sub>2</sub> in the  
357 gas-phase formation of HO<sub>2</sub>· H<sub>2</sub>O and HO<sub>2</sub>· NH<sub>3</sub> complexes, *International Journal of Chemical Kinetics*, 9, 875-885,  
358 1977.

359 He, S. Z., Chen, Z. M., Zhang, X., Zhao, Y., Huang, D. M., Zhao, J. N., Zhu, T., Hu, M., and Zeng, L. M.: Measurement of  
360 atmospheric hydrogen peroxide and organic peroxides in Beijing before and during the 2008 Olympic Games: Chemical  
361 and physical factors influencing their concentrations, *J Geophys Res-Atmos*, 115, Artn D1730710.1029/2009jd013544,  
362 2010.

363 Heland, J., Kleffmann, J., Kurtenbach, R., and Wiesen, P.: A new instrument to measure gaseous nitrous acid (HONO) in the  
364 atmosphere, *Environ. Sci. Technol.*, 35, 3207–3212, <https://doi.org/10.1021/es000303t>, 2001

365 Herrmann, H., Schaefer, T., Tilgner, A., Styler, S. A., Weller, C., Teich, M., and Otto, T.: Tropospheric Aqueous-Phase  
366 Chemistry: Kinetics, Mechanisms, and Its Coupling to a Changing Gas Phase, *Chem Rev*, 115, 4259-4334, 2015.

367 Hoffmann, M., and Edwards, J.: Kinetics of the oxidation of sulfite by hydrogen peroxide in acidic solution, *The Journal of*  
368 *Physical Chemistry*, 79, 2096-2098, 1975.

369 Hua, W., Chen, Z. M., Jie, C. Y., Kondo, Y., Hofzumahaus, A., Takegawa, N., Chang, C. C., Lu, K. D., Miyazaki, Y., Kita,  
370 K., Wang, H. L., Zhang, Y. H., and Hu, M.: Atmospheric hydrogen peroxide and organic hydroperoxides during PRIDE-

371 PRD'06, China: their concentration, formation mechanism and contribution to secondary aerosols, *Atmos Chem Phys*, 8,  
372 6755-6773, DOI 10.5194/acp-8-6755-2008, 2008.

373 Kleinman, L. I.: Photochemical formation of peroxides in the boundary layer, *Journal of Geophysical Research:*  
374 *Atmospheres*, 91, 10889-10904, 1986.

375 Lee, M., Heikes, B. G., Jacob, D. J., Sachse, G., and Anderson, B.: Hydrogen peroxide, organic hydroperoxide, and  
376 formaldehyde as primary pollutants from biomass burning, *Journal of Geophysical Research: Atmospheres*, 102, 1301-  
377 1309, 10.1029/96jd01709, 1997.

378 Lee, M., Kie, J. A., Kim, Y. M., and Lee, G.: Characteristics of atmospheric hydrogen peroxide variations in Seoul megacity  
379 during 2002-2004, *Sci Total Environ*, 393, 299-308, 10.1016/j.scitotenv.2007.11.037, 2008.

380 Lee, M. H., Heikes, B. G., and O'Sullivan, D. W.: Hydrogen peroxide and organic hydroperoxide in the troposphere: A  
381 review, *Atmos Environ*, 34, 3475-3494, Doi 10.1016/S1352-2310(99)00432-X, 2000.

382 Liang, H., Chen, Z. M., Huang, D., Zhao, Y., and Li, Z. Y.: Impacts of aerosols on the chemistry of atmospheric trace gases:  
383 a case study of peroxides and HO<sub>2</sub> radicals, *Atmos Chem Phys*, 13, 11259-11276, 10.5194/acp-13-11259-2013, 2013.

384 Liu, M. X., Song, Y., Yao, H., Kang, Y. N., Li, M. M., Huang, X., and Hu, M.: Estimating emissions from agricultural fires  
385 in the North China Plain based on MODIS fire radiative power, *Atmos Environ*, 112, 326-334, 2015.

386 Liu, P. F., Zhang, C. L., Xue, C. Y., Mu, Y. J., Liu, J. F., Zhang, Y. Y., Tian, D., Ye, C., Zhang, H. X., and Guan, J.: The  
387 contribution of residential coal combustion to atmospheric PM<sub>2.5</sub> in northern China during winter, *Atmos Chem Phys*, 17,  
388 11503-11520, 10.5194/acp-17-11503-2017, 2017.

389 Liu, P., Ye, C., Zhang, C., He, G., Xue, C., Liu, J., Liu, C., Zhang, Y., Song, Y., Li, X., Wang, X., Chen, J., He, H.,  
390 Herrmann, H., and Mu, Y.: Photochemical Aging of Atmospheric Fine Particles as a Potential Source for Gas-Phase  
391 Hydrogen Peroxide, *Environ Sci Technol*, 10.1021/acs.est.1c04453, 2021.

392 Liu, Y., Lu, K., Li, X., Dong, H., Tan, Z., Wang, H., Zou, Q., Wu, Y., Zeng, L., Hu, M., Min, K.-E., Kecorius, S.,  
393 Wiedensohler, A., and Zhang, Y.: A Comprehensive Model Test of the HONO Sources Constrained to Field  
394 Measurements at Rural North China Plain, *Environ Sci Technol*, 53, 3517-3525, 10.1021/acs.est.8b06367, 2019.

395 Ma, X. F., Tan, Z. F., Lu, K. D., Yang, X. P., Liu, Y. H., Li, S. L., Li, X., Chen, S. Y., Novelli, A., Cho, C. M., Zeng, L. M.,  
396 Wahner, A., and Zhang, Y. H.: Winter photochemistry in Beijing: Observation and model simulation of OH and HO<sub>2</sub>  
397 radicals at an urban site, *Sci Total Environ*, 685, 85-95, 2019.

398 Nel, A.: Air pollution-related illness: Effects of particles, *Science*, 308, 804-806, 10.1126/science.1108752, 2005.

399 Nunnermacker, L. J., Weinstein-Lloyd, J. B., Hillery, B., Giebel, B., Kleinman, L. I., Springston, S. R., Daum, P. H.,  
400 Gaffney, J., Marley, N., and Huey, G.: Aircraft and ground-based measurements of hydroperoxides during the 2006  
401 MILAGRO field campaign, *Atmos Chem Phys*, 8, 7619-7636, 10.5194/acp-8-7619-2008, 2008.

402 Penkett, S. A., Jones, B. M. R., Brice, K. A., and Eggleton, A. E. J.: Importance of Atmospheric Ozone and Hydrogen-  
403 Peroxide in Oxidizing Sulfur-Dioxide in Cloud and Rainwater, *Atmos Environ*, 13, 123-137, Doi 10.1016/0004-  
404 6981(79)90251-8, 1979.

405 Poschl, U., and Shiraiwa, M.: Multiphase Chemistry at the Atmosphere-Biosphere Interface Influencing Climate and Public  
406 Health in the Anthropocene, *Chem Rev*, 115, 4440-4475, 2015.

407 Qin, M., Chen, Z., Shen, H., Li, H., Wu, H., and Wang, Y.: Impacts of heterogeneous reactions to atmospheric peroxides:  
408 Observations and budget analysis study, *Atmos Environ*, 183, 144-153, 10.1016/j.atmosenv.2018.04.005, 2018.

409 Reeves, C. E., and Penkett, S. A.: Measurements of peroxides and what they tell us, *Chem Rev*, 103, 5199-5218,  
410 10.1021/cr0205053, 2003.

411 Sillman, S.: The use of NO<sub>y</sub>, H<sub>2</sub>O<sub>2</sub>, and HNO<sub>3</sub> as indicators for ozone-NO<sub>x</sub>-hydrocarbon sensitivity in urban locations,  
412 *Journal of Geophysical Research: Atmospheres*, 100, 14175-14188, 1995.

413 Sillman, S., He, D., Pippin, M. R., Daum, P. H., Imre, D. G., Kleinman, L. I., Lee, J. H., and Weinstein-Lloyd, J.: Model  
414 correlations for ozone, reactive nitrogen, and peroxides for Nashville in comparison with measurements: Implications for  
415 O<sub>3</sub>-NO<sub>x</sub>-hydrocarbon chemistry, *Journal of Geophysical Research: Atmospheres*, 103, 22629-22644, 1998.

416 Slater, E. J., Whalley, L. K., Woodward-Massey, R., Ye, C. X., Lee, J. D., Squires, F., Hopkins, J. R., Dunmore, R. E.,  
417 Shaw, M., Hamilton, J. F., Lewis, A. C., Crilley, L. R., Kramer, L., Bloss, W., Vu, T., Sun, Y. L., Xu, W. Q., Yue, S. Y.,  
418 Ren, L. J., Acton, W. J. F., Hewitt, C. N., Wang, X. M., Fu, P. Q., and Heard, D. E.: Elevated levels of OH observed in

419 haze events during wintertime in central Beijing, *Atmos Chem Phys*, 20, 14847-14871, 10.5194/acp-20-14847-2020,  
420 2020.

421 Stockwell, W. R., Kirchner, F., Kuhn, M., and Seefeld, S.: A new mechanism for regional atmospheric chemistry modeling,  
422 *J Geophys Res-Atmos*, 102, 25847-25879, 1997.

423 Su, H., Cheng, Y. F., Oswald, R., Behrendt, T., Trebs, I., Meixner, F. X., Andreae, M. O., Cheng, P., Zhang, Y., and Poschl,  
424 U.: Soil Nitrite as a Source of Atmospheric HONO and OH Radicals, *Science*, 333, 1616-1618, 2011.

425 Tan, Z. F., Fuchs, H., Lu, K. D., Hofzumahaus, A., Bohn, B., Broch, S., Dong, H. B., Gomm, S., Haseler, R., He, L. Y.,  
426 Holland, F., Li, X., Liu, Y., Lu, S. H., Rohrer, F., Shao, M., Wang, B. L., Wang, M., Wu, Y. S., Zeng, L. M., Zhang, Y. S.,  
427 Wahner, A., and Zhang, Y. H.: Radical chemistry at a rural site (Wangdu) in the North China Plain: observation and  
428 model calculations of OH, HO<sub>2</sub> and RO<sub>2</sub> radicals, *Atmos Chem Phys*, 17, 663-690, 10.5194/acp-17-663-2017, 2017.

429 Tan, Z., Lu, K., Jiang, M., Su, R., Dong, H., Zeng, L., Xie, S., Tan, Q., and Zhang, Y.: Exploring ozone pollution in  
430 Chengdu, southwestern China: A case study from radical chemistry to O<sub>3</sub>-VOC-NO<sub>x</sub> sensitivity, *Sci Total Environ*, 636,  
431 775-786, <https://doi.org/10.1016/j.scitotenv.2018.04.286>, 2018.

432 Vermeuel, M. P., Novak, G. A., Alwe, H. D., Hughes, D. D., Kaleel, R., Dickens, A. F., Kenski, D., Czarnetzki, A. C.,  
433 Stone, E. A., and Stanier, C. O.: Sensitivity of Ozone Production to NO<sub>x</sub> and VOC Along the Lake Michigan Coastline,  
434 *Journal of Geophysical Research: Atmospheres*, 124, 10989-11006, 2019.

435 Walker, S. J., Evans, M. J., Jackson, A. V., Steinbacher, M., Zellweger, C., and McQuaid, J. B.: Processes controlling the  
436 concentration of hydroperoxides at Jungfraujoch Observatory, Switzerland, *Atmos Chem Phys*, 6, 5525-5536, DOI  
437 10.5194/acp-6-5525-2006, 2006.

438 Wang, X., Gemayel, R., Hayeck, N., Perrier, S., Charbonnel, N., Xu, C., Chen, H., Zhu, C., Zhang, L., and Wang, L.:  
439 Atmospheric photosensitization: a new pathway for sulfate formation, *Environ Sci Technol*, 2020.

440 Wang, Y., Chen, Z. M., Wu, Q. Q., Liang, H., Huang, L. B., Li, H., Lu, K. D., Wu, Y. S., Dong, H. B., Zeng, L. M., and  
441 Zhang, Y. H.: Observation of atmospheric peroxides during Wangdu Campaign 2014 at a rural site in the North China  
442 Plain, *Atmos Chem Phys*, 16, 10985-11000, 10.5194/acp-16-10985-2016, 2016.



443 Wang, Y. X., Zhang, Q. Q., Jiang, J. K., Zhou, W., Wang, B. Y., He, K. B., Duan, F. K., Zhang, Q., Philip, S., and Xie, Y.  
444 Y.: Enhanced sulfate formation during China's severe winter haze episode in January 2013 missing from current models, *J*  
445 *Geophys Res-Atmos*, 119, 2014.

446 Watanabe, K., Yachi, C., Nishibe, M., Michigami, S., Saito, Y., Eda, N., Yamazaki, N., and Hirai, T.: Measurements of  
447 atmospheric hydroperoxides over a rural site in central Japan during summers using a helicopter, *Atmos Environ*, 146,  
448 174-182, 10.1016/j.atmosenv.2016.06.074, 2016.

449 Watanabe, K., Yachi, C., Song, X. J., Kakuyama, S., Nishibe, M., and Michigami, S.: Measurements of atmospheric  
450 hydroperoxides at a rural site in central Japan, *J Atmos Chem*, 75, 71-84, 2018.

451 Watson, J. G., Chow, J. C., and Houck, J. E.: PM<sub>2.5</sub> chemical source profiles for vehicle exhaust, vegetative burning,  
452 geological material, and coal burning in Northwestern Colorado during 1995, *Chemosphere*, 43, 1141-1151, 2001.

453 Wiedinmyer, C., Akagi, S. K., Yokelson, R. J., Emmons, L. K., Al-Saadi, J. A., Orlando, J. J., and Soja, A. J.: The Fire  
454 INventory from NCAR (FINN): a high resolution global model to estimate the emissions from open burning, *Geosci.*  
455 *Model Dev.*, 4, 625-641, 10.5194/gmd-4-625-2011, 2011.

456 Xue, C., Ye, C., Zhang, Y., Ma, Z., Liu, P., Zhang, C., Zhao, X., Liu, J., and Mu, Y.: Development and application of a twin  
457 open-top chambers method to measure soil HONO emission in the North China Plain, *Sci Total Environ*, 659, 621-631,  
458 2019.

459 Xue, C., Ye, C., Zhang, C., Catoire, V., Liu, P., Gu, R., Zhang, J., Ma, Z., Zhao, X., Zhang, W., Ren, Y., Krysztofiak, G.,  
460 Tong, S., Xue, L., An, J., Ge, M., Mellouki, A., and Mu, Y.: Evidence for Strong HONO Emission from Fertilized  
461 Agricultural Fields and its Remarkable Impact on Regional O<sub>3</sub> Pollution in the Summer North China Plain, *ACS Earth*  
462 *and Space Chemistry*, 10.1021/acsearthspacechem.0c00314, 2021.

463 Xue, C. Y., Zhang, C. L., Ye, C., Liu, P. F., Catoire, V., Krysztofiak, G., Chen, H., Ren, Y. G., Zhao, X. X., Wang, J. H.,  
464 Zhang, F., Zhang, C. X., Zhang, J. W., An, J. L., Wang, T., Chen, J. M., Kleffmann, J., Mellouki, A., and Mu, Y. J.:  
465 HONO Budget and Its Role in Nitrate Formation in the Rural North China Plain, *Environ Sci Technol*, 54, 11048-11057,  
466 2020.

467 Xue, J., Yuan, Z. B., Griffith, S. M., Yu, X., Lau, A. K. H., and Yu, J. Z.: Sulfate Formation Enhanced by a Cocktail of High  
468 NO<sub>x</sub>, SO<sub>2</sub>, Particulate Matter, and Droplet pH during Haze-Fog Events in Megacities in China: An Observation-Based  
469 Modeling Investigation, *Environ Sci Technol*, 50, 7325-7334, 2016.

470 Ye, C., Liu, P., Ma, Z., Xue, C., Zhang, C., Zhang, Y., Liu, J., Liu, C., Sun, X., and Mu, Y.: High H<sub>2</sub>O<sub>2</sub> Concentrations  
471 Observed during Haze Periods during the Winter in Beijing: Importance of H<sub>2</sub>O<sub>2</sub> Oxidation in Sulfate Formation,  
472 *Environmental Science & Technology Letters*, 10.1021/acs.estlett.8b00579, 2018.

473 Ye, C., Chen, H., Hoffmann, E. H., Mettke, P., Tilgner, A., He, L., Mutzel, A., Brüggemann, M., Poulain, L., and Schaefer,  
474 T.: Particle-Phase Photoreactions of HULIS and TMI<sub>s</sub> Establish a Strong Source of H<sub>2</sub>O<sub>2</sub> and Particulate Sulfate in the  
475 Winter North China Plain, *Environ Sci Technol*, 2021.

476 Yokelson, R. J., Crounse, J. D., DeCarlo, P. F., Karl, T., Urbanski, S., Atlas, E., Campos, T., Shinozuka, Y., Kapustin, V.,  
477 Clarke, A. D., Weinheimer, A., Knapp, D. J., Montzka, D. D., Holloway, J., Weibring, P., Flocke, F., Zheng, W., Toohey,  
478 D., Wennberg, P. O., Wiedinmyer, C., Mauldin, L., Fried, A., Richter, D., Walega, J., Jimenez, J. L., Adachi, K., Buseck,  
479 P. R., Hall, S. R., and Shetter, R.: Emissions from biomass burning in the Yucatan, *Atmos. Chem. Phys.*, 9, 5785-5812,  
480 10.5194/acp-9-5785-2009, 2009.

481 Yu, D., Tan, Z., Lu, K., Ma, X., Li, X., Chen, S., Zhu, B., Lin, L., Li, Y., Qiu, P., Yang, X., Liu, Y., Wang, H., He, L.,  
482 Huang, X., and Zhang, Y.: An explicit study of local ozone budget and NO<sub>x</sub>-VOCs sensitivity in Shenzhen China, *Atmos*  
483 *Environ*, 224, 117304, <https://doi.org/10.1016/j.atmosenv.2020.117304>, 2020.

484 Zhang, Q., Liu, J., He, Y., Yang, J., Gao, J., Liu, H., Tang, W., Chen, Y., Fan, W., and Chen, X.: Measurement of hydrogen  
485 peroxide and organic hydroperoxide concentrations during autumn in Beijing, China, *J Environ Sci-China*, 64, 72-81,  
486 2018.

487 Zhang, Y., Bao, F., Li, M., Xia, H., Huang, D., Chen, C., and Zhao, J.: Photoinduced Uptake and Oxidation of SO<sub>2</sub> on  
488 Beijing Urban PM<sub>2.5</sub>, *Environ Sci Technol*, 10.1021/acs.est.0c01532, 2020.

489 Zheng, B., Zhang, Q., Zhang, Y., He, K. B., Wang, K., Zheng, G. J., Duan, F. K., Ma, Y. L., and Kimoto, T.: Heterogeneous  
490 chemistry: a mechanism missing in current models to explain secondary inorganic aerosol formation during the January  
491 2013 haze episode in North China, *Atmos Chem Phys*, 15, 2031-2049, 10.5194/acp-15-2031-2015, 2015.

492 Zuo, Y., and Hoigné, J.: Evidence for photochemical formation of H<sub>2</sub>O<sub>2</sub> and oxidation of SO<sub>2</sub> in authentic fog water,  
493 Science, 260, 71-73, 1993.